Correlation of the resistive switching and polarization switching in zinc oxide thin films using scanning probe microscopy techniques

Juanxiu Xiao and Kaiyang Zeng[a)]
Department of Mechanical Engineering, National University of Singapore, 117576, Singapore

Lai-Mun Wong and Shijie Wang
*Institute of Materials Research and Engineering (IMRE), Agency for Science, Technology and Research (A*STAR), 117602, Singapore*

(Received 30 March 2015; accepted 28 September 2015)

In this study, resistive switching (RS), polarization switching, and charge distribution under DC bias in undoped ZnO thin films are studied by applying scanning probe microscopy (SPM) techniques on the same location. The techniques include Piezoresponce Force Microscopy, Kelvin Probe Force Microscopy, and Conductive Atomic Force Microscopy. The effects of oxygen partial pressure during the film deposition are also investigated. The results show that high resistance state (HRS) is accompanied by the polarization switching and charges storage. By comparing the SPMs results from the same location, it is found that the oxygen partial pressure during film deposition is an important factor over the holes injection during the poling processes in the HRS. On the other hand, the low resistance state (LRS) may be dominated by the electrons injection. Based on these findings, the energy band diagrams in the Pt-tip/ZnO-film/Pt-bottom-electrode structure with the applications of the external biases are illustrated schematically. This study also proposes a more persuasive mechanism of RS in ZnO films.

I. INTRODUCTION

Nonvolatile Random Access Memories (RAMs) have been developed for data storage applications with higher storage and readout speed; higher data density and lower power consumptions. The RAMs include several categories, such as ferroelectric RAMs (FRAMs), magnetic RAMs (MRAMs), resistive RAMs (RRAMs), and so on.[1–7] Generally-speaking, FRAMs and MRAMs have limitations in overcoming the scaling problems,[8,9] whereas RRAMs can overcome this limit and achieve a higher storage density. Therefore, RRAMs have been studied extensively in recent years. ZnO-based oxide materials, such as nanorods,[10–12] nanowires,[13] thin films,[14–18] nanocolumns[19], and nanoislands,[20] are considered to be the promising materials for RRAMs applications. In most of those studies, Pt is used as top and/or bottom electrodes, it can form Schottky contact at the Pt/ZnO interface due to the differences in the work functions between Pt and ZnO.[21] In addition, Pt can also act as catalyst for oxygen gas decomposition.[22] The possible mechanisms underlying the resistive switching (RS) behavior have also been proposed. One of which is a conductive filament model in which conducting filamentary paths are formed and ruptured between the two electrodes or in a close vicinity of the electrode/film interface. Another one is the charge trap model in which the resistivity is modified by the defects engineering in film or trapped carrier in electrode/film interface under an electric field.[1,2,8] For ZnO-based materials, the ferroelectric-like property[23] might further complicate the RS behavior; the polarization reversal might also change the conduction band profile in the electrode/material interface and results in RS phenomena.[24,25] However, these phenomena have not been studied in detail yet. During the studies of the RS behavior, Scanning Probe Microscopy (SPM) techniques are widely used.[8,26,27] For example, conductive Atomic Force Microscopy (c-AFM) has been used to characterize the changes of the conductivity,[16,28] whereas Piezoresponse Force Microscopy (PFM) is used to study the polarization switching at micro-to nano-scales.[29,30] The c-AFM technique is operated in contact mode. By using this technique, the topography and current images of the area scanned by the c-AFM tip can be obtained simultaneously; the changes of current with the applied bias can be used to construct the current–voltage (*I–V*) curve, hence the RS behavior can be determined. In addition, Kelvin Probe Force Microscopy (KPFM) technique can be used to measure the surface potential and hence quantitatively analyzed the dynamic changes of the relative amounts of polarization charges, injection charges, and screen charges.[31,32]

Recently, Qi and colleagues combined the c-AFM and PFM techniques to study the RS of the self-assembled

Contributing Editor: José Arana Varela
[a)]Address all correspondence to this author.
e-mail: mpezk@nus.edu.sg
DOI: 10.1557/jmr.2015.310

 © Materials Research Society 2015

https://doi.org/10.1557/jmr.2015.310 Published online by Cambridge University Press

single-crystalline ZnO nano-island deposited on silicon substrate.[20] Furthermore, Herng and colleagues also reported that, when ZnO film was switched to high resistance state (HRS), the polarization switching behavior was observed.[16] However, up to now, the RS and polarization switching were only correlated in the global scale. The mechanisms of RS were also not discussed. In addition, their study also proposed the importance of the oxygen vacancies for the polarization switching, but the effects to the RS have not been studied. Therefore, in this study, the correlation between the RS and polarization switching is studied by applying various SPM techniques on the same location of the sample surface. First, poling processes with a sequence DC biases are applied on a larger square area by using the c-AFM technique so that this area is switched to HRS; then the same area (under HRS) is scanned by using the PFM technique so that the polarization switching processes can be studied. At the same time, the KPFM technique is applied on the same area to characterize the charge distribution in relationship to the RS behavior in ZnO film. For those experiments, undoped ZnO thin films are deposited by Pulse Laser Deposition (PLD) technique under oxygen deficient environment. It is well known that undoped ZnO thin films which are grown in an oxygen deficient environment can exhibit the mechanisms of the impurity band conduction.[33] Therefore, the effects of the oxygen partial pressure during the film deposition on RS behavior are also studied in this work.

II. MATERIALS AND EXPERIMENTS

In this work, the undoped ZnO thin film samples (with an approximately thickness of 36 nm) were deposited on commercial Pt/Ti/SiO_2/Si substrate by PLD technique with the laser parameters of a frequency of 20 Hz and an energy fluence of 3 J/cm^2. The substrate was commercial Si wafer with 300 nm silicon oxide layer, 50 nm Ti layer, and finally with 150 nm Pt layer (Addision Engineering Inc., San Jose, California) served as bottom electrode for various SPM characterizations. The substrate temperature was 350 °C during the film deposition. The samples were deposited under oxygen partial pressure (P_{O_2}) of 1.2×10^{-4} and 1.6×10^{-2} Torr, respectively. The x-ray diffraction was used to characterize the samples' crystallinity and crystallographic orientation. The results confirmed that the ZnO films used in this work have fully crystallinity and oriented with the *c*-axis along the (002) direction (Fig. S1—Supporting Information).

A commercial SPM system (MFP-3D, Asylum Research, Santa Barbara, California) was used in this work. The system is equipped with a commercial software platform (Igor Pro 6.22A; WaveMetrics, Inc., Lake Osuego, Oregon) and SPM control software (Asylum Research, version 101010-2106). The PFM technique was used to obtain the piezoresponse phase and amplitude images. The PFM amplitude image shows the deformation due to the inverse piezoelectric effect; and phase image can yield the information of the polarization direction below the tip in relative to the direction of the applied electric field. In addition, the PFM technique includes both vertical PFM (the electric field is aligned parallel to the measured deformation) and lateral PFM (electric field is applied orthogonal to the measured deformation). In this work, only vertical PFM technique was used. For the vertical PFM technique, phase angles equal to either 0° or 180°, indicating that the polarization vector points either downward to the bottom electrode or upward to the sample surface. To study the polarization switching behavior, Piezoresponse Force Spectroscopy (PFS) experiments were conducted. In the PFS experiments, the SPM tip was fixed at an arbitrary location and a bias-induced remnant polarization was acquired. Using this technique, phase hysteresis loop $\phi(E)$ and amplitude loop $A(E)$ were obtained. The piezoresponse hysteresis loop PR(E) was then calculated with the equation $PR(E) = A(E)^{*}\cos[\phi(E)]$ at bias-off state. With the piezoresponse hysteresis loop, the negative and positive coercive voltages were determined.

The KPFM measurement is conducted in the alternating contact mode (also called tapping mode in some SPM systems). In this study, all of the KPFM images were acquired by applying an AC voltage of 3 V with delta height and start delta height of 40 nm, which were the same as those used in the previous work.[34] Due to the set-up of the SPM equipment, during the PFM and KPFM measurements, the biases are applied through the SPM tips whereas the samples are grounded through the bottom electrode [Fig. 1(a)].

In the c-AFM measurement, the same SPM system with the conductive AFM module (ORCA, Asylum Research) was used. Several c-AFM experiments were conducted. First, a series DC voltages was applied so that the topography and current images were simultaneously obtained on the 256 × 256 points array. When plotting the *I–V* curve as the function of the applied DC voltage (*V*), the average current (*I*) was obtained by averaging current values of every point in the current image.

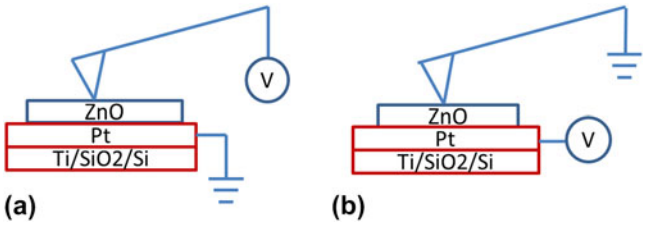


FIG. 1. Schematic drawing of the SPM set-up used in this study; (a) for PFM and KPFM measurements, the bias is applied to the SPM tip, whereas the sample is grounded through the bottom electrode (Pt); (b) for c-AFM measurement, the bias is applied to the sample through the bottom electrode (Pt), whereas the SPM tip is grounded.

https://doi.org/10.1557/jmr.2015.310 Published online by Cambridge University Press

After the confirmation of the RS behavior, the sequence DC bias processes with different scanning rates (1 and 0.2 Hz) were applied to the sample surface, this experiment was used to determine the conditions for RS in the ZnO samples. In all of the c-AFM measurements, the set point, i.e., the loading force was kept as a constant. Again, due to the set-up of the SPM equipment, during the c-AFM measurement, the bias is applied to the bottom electrode of the sample whereas the tip is grounded [Fig. 1(b)]. In all of the PFM, KPFM, and c-AFM measurements, commercially available Pt-coated Si tips (AC240TM; Olympus, Tokyo, Japan) were used. The tips had average tip radius of 15 nm, average stiffness of 2 N/m, and average resonance frequency of 70 kHz, respectively.

III. RESULTS AND DISCUSSION

A. RS characteristics

In this work, the average current–voltage (*I–V*) curves of the ZnO samples are measured in the same way as reported previously.[16] As the method to obtain the average *I–V* curves is similar to what reported in the previous study,[16] it is therefore not reported in this paper. These *I–V* curves are shown as Figs. S2 and S3 (Supplementary Information) for the ZnO samples deposited under the oxygen partial pressures of $P_{O_2} = 1.2 \times 10^{-4}$ and 1.6×10^{-2} Torr, respectively. These *I–V* curves confirms the RS behavior in ZnO samples. It is found that the "set" voltage is approximately 3.5 V, whereas the "reset" voltage is about −3.5 V. Following this, PFS technique is used to determine the coercive voltage for polarization reversal (the detail of the experiments are not shown here). The results are shown in Fig. 2. The results show the coercive voltage for the polarization reversal is ±2.5 V.

After determination of the average *I–V* curves and coercive voltage for ZnO film, the RS of the undoped ZnO film (deposited under $P_{O_2} = 1.2 \times 10^{-4}$ Torr) is studied by DC poling experiments using the c-AFM technique. During the poling experiments, DC biases with different polarities are applied in sequence to the sample surface [Fig. 3(a)], i.e., a 3×3 μm^2 area is first poled with −10 V DC bias [Fig. 3(b)], and then the central 1×1 μm^2 area is poled with 10 V DC bias [Fig. 3(c)]. After these poling processes, a 5×5 μm^2 area which includes these poled areas is scanned with c-AFM under 0.5 V. It is found that this small DC bias, 0.5 V used for the c-AFM scanning, neither changes the film conductance as the "set" voltage is 3.5 V; nor perturbs the domain state as 0.5 V bias cannot switch the domain, as the scanning voltage is less than the voltage for polarization reversal (±2.5 V) (Fig. 2). Hereafter, the read-out voltage used in this work for c-AFM scanning is 0.5 V. To confirm whether the switching behavior in ZnO film can be maintained, the poling processes are conducted with two rates, 1 and 0.2 Hz [Figs. 2(d) and 2(e)]. It is interesting to find that, independent of the poling rate, when biases are on, the area poled by −10 V shows no current [Fig. 3(b)], whereas the area poled by 10 V shows high current [Fig. 3(c)]. Hence, during the poling processes, the area poled by −10 V has switched to HRS whereas the area poled by 10 V has switched to low resistance state (LRS). However, after the poling processes, when the area is scanned with 0.5 V by the c-AFM technique, the situation becomes very different. It is found that, when the areas are poled with 1 Hz, after the poling processes, the area poled by −10 V is maintained at HRS, but the area poled by 10 V is switched back to HRS [Fig. 3(e)], indicating that the LRS cannot be maintained if the poling rate is high. On the other hand, when the areas are poled under 0.2 Hz, both HRS and LRS are maintained after the poling processes [Fig. 3(d)]. This suggests that the ZnO films may have similar behavior as the nonvolatile RS. It also suggests that the switched states in ZnO can only be maintained at the slow poling rate. This may have important implication on how the ZnO film should be used for the data storage applications.

B. Correlation of RS behavior with polarization reversal

The areas poled by the c-AFM technique are then scanned using the PFM technique in the same SPM system. This experiment is similar to the work by Yang and colleagues on Ca-doped $BiFeO_3$ film.[24] Figures 4(a) and 4(b) are the current image and the vertical PFM phase image of the same area after the poling processes induced by c-AFM, respectively (the poling rate by c-AFM is 0.2 Hz on the ZnO film of $P_{O_2} = 1.2 \times 10^{-4}$ Torr). It is noticed that when the sample is switched to HRS by −10 V, the polarization direction is also switched by more than 150° (from yellow color to purple color in the red box), on the other hand, the 10 V poling has switched the sample from HRS to LRS, but cannot switch the polarization directions [green box in Fig. 4(b)], in addition, the line profile [Fig. 4(c)] also shows that there is no observable differences in the polarization angles between the red and green boxes. However, when poling is conducted at 1 Hz rate, as the LRS cannot be maintained and has been switched back to HRS after the poling bias is removed, it is found that the polarization within the green box has also been switched back to the angle similar to the unpoled region (from purple color to yellow color), this is also confirmed by the line profile [Fig. 4(f)]. These results have further confirmed that the polarization switching only occurs at HRS, whereas LRS cannot cause polarization switching.

To study the effects of oxygen partial pressure to the polarization reversal, the same poling processes are also

https://doi.org/10.1557/jmr.2015.310 Published online by Cambridge University Press

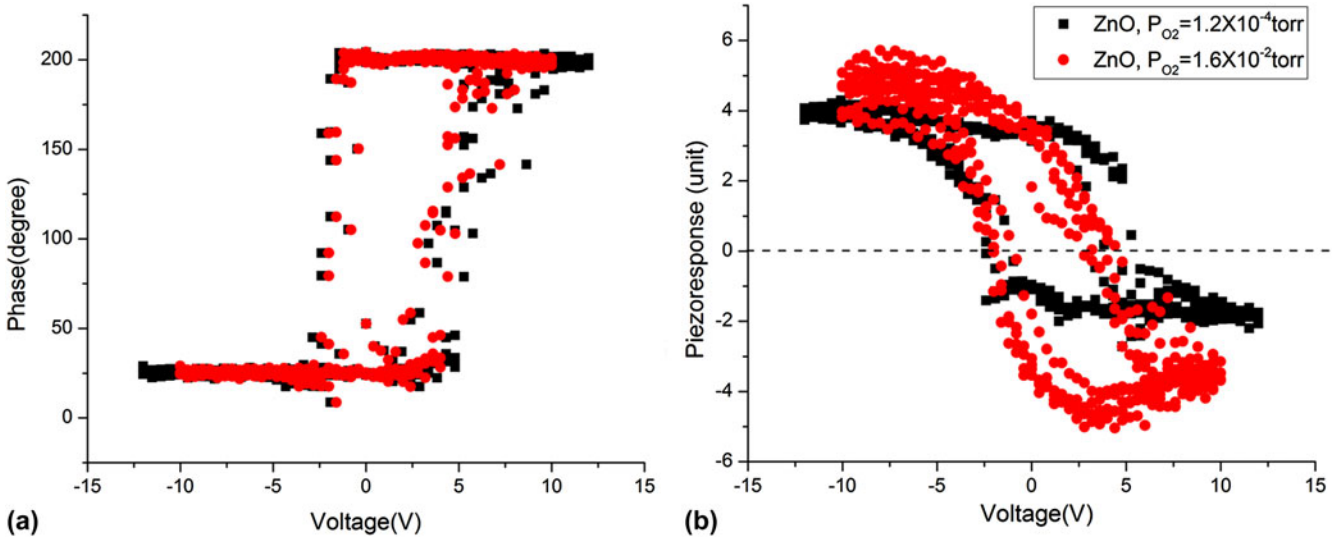


FIG. 2. (a) Phase loops measured by PFS measurements; and (b) piezoresponse hysteresis loops (calculated from PR(E) = A(E) * cos[ϕ(E)]) for ZnO thin films deposited under two different oxygen partial pressures: $P_{O_2} = 1.2 \times 10^{-4}$ Torr and $P_{O_2} = 1.6 \times 10^{-2}$ Torr, respectively.

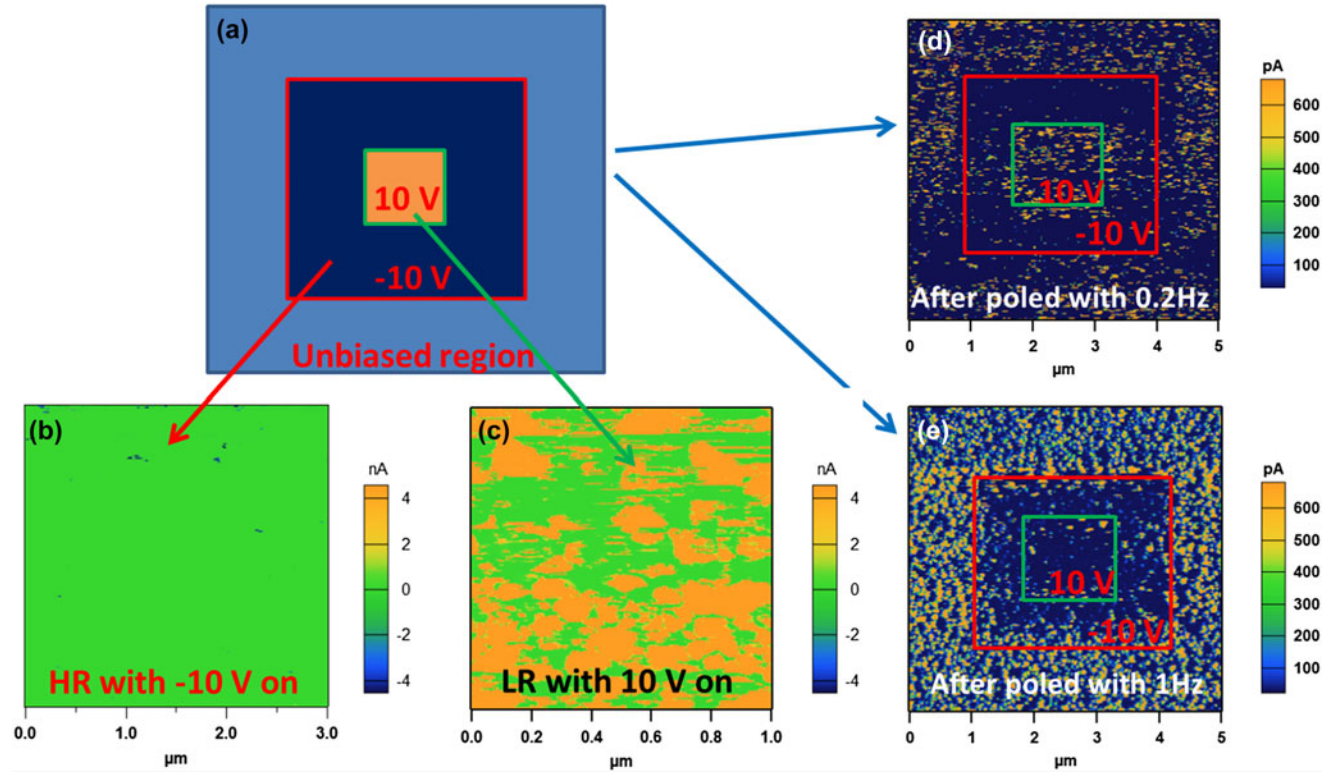


FIG. 3. (a) Schematic diagram showing the poling processes (−10 and 10 V) for ZnO film sample; (b) current image from a 3 × 3 μm^2 area poled by −10 V bias; (c) current image from the middle 1 × 1 μm^2 area poled by 10 V bias; (d) current image of 5 × 5 μm^2 area by these poling processes with 0.2 Hz rate; and (e) current image of 5 × 5 μm^2 area by these poling processes with 1 Hz rate; the read out voltage is 0.5 V for all of the current images.

conducted on the film deposited at oxygen partial pressure of $P_{O_2} = 1.6 \times 10^{-2}$ Torr with the tip bias. Figures 5(a) and 5(b) are the vertical PFM phase images for the two films deposited at different oxygen partial pressures, i.e., a poling process with −10 V tip bias is first applied to a 3 × 3 μm^2 area (red square) and then a subsequent poling process with 10 V tip bias is applied to the central 1 × 1 μm^2 area (green square). It is observed that, under the tip-biased poling processes, the polarization switching occurs under HRS in both films.

https://doi.org/10.1557/jmr.2015.310 Published online by Cambridge University Press

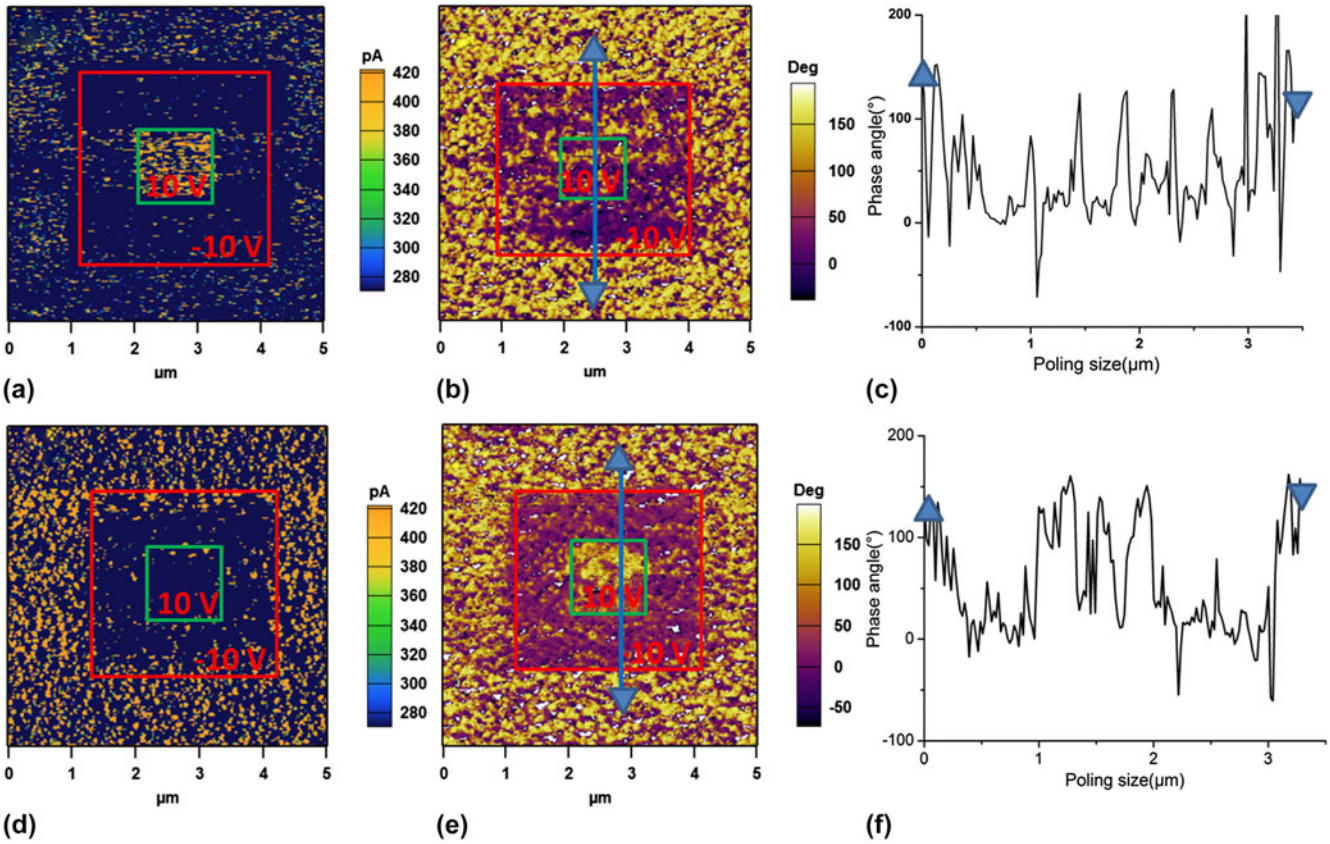


FIG. 4. (a) Current image after the DC poling processes (illustrated as in Fig. 3) (with the scan rate is 0.2 Hz) on ZnO film deposited under $P_{O_2} = 1.2 \times 10^{-4}$ Torr; (b) out-of-plane PFM phase image of the same area [shown in (a)] after the c-AFM measurement; (c) line profiles of the out-of-plane PFM phase image from the line section marked in (b); (d) c-AFM current image after the same DC poling processes (with the scan rate is 1 Hz) on the same film; (e) out-of-plane PFM phase image of the same area [as shown in (d)] after the c-AFM measurement; and (f) line profiles of the out-of-plane PFM phase image from the line section marked in (e).

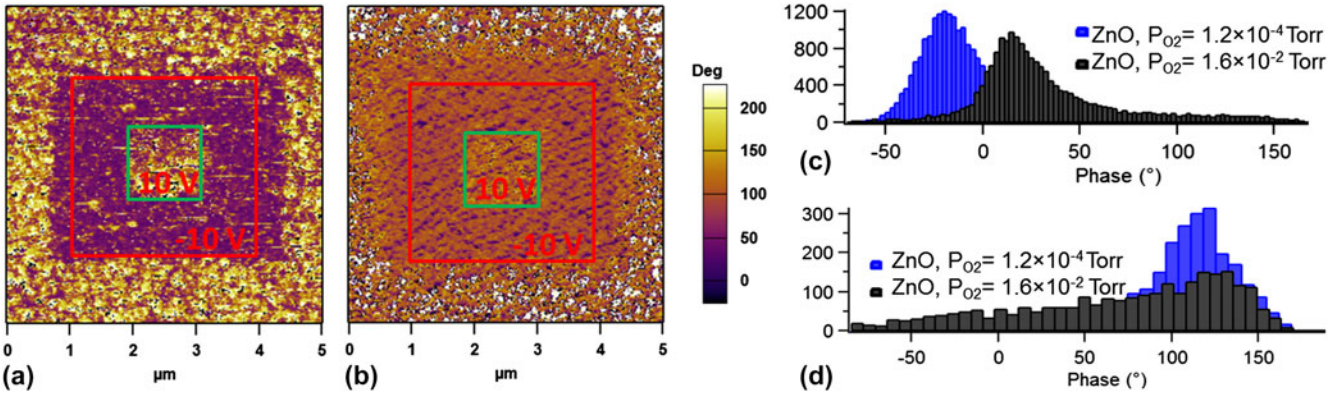


FIG. 5. (a) and (b) are the out-of-plane phase images after the DC poling processes (illustrated as in Fig. 3) for ZnO films deposited under $P_{O_2} = 1.2 \times 10^{-4}$ Torr and $P_{O_2} = 1.6 \times 10^{-2}$ Torr, respectively; (c) phase histogram from the red marked squares (are poled by -10 V) for two samples; and (d) phase histogram from the green marked squares (area poled by 10 V) for two samples.

Figure 5(a) is the PFM phase image, which is obtained after the tip biased poling processes. It shows the similar results as that of the Fig. 4(b) which is obtained after poling processes with the sample bias, and hence this can exclude the effects of the different contact areas at the bottom-electrode/thin-film interface and tip/thin-film interface during the poling between the tip bias and sample bias. Under the same poling processes and conditions, the polarization reversal of ZnO film deposited under $P_{O_2} = 1.2 \times 10^{-4}$ Torr [Fig. 5(a)] is more clear and

https://doi.org/10.1557/jmr.2015.310 Published online by Cambridge University Press

obvious than that of the ZnO film deposited under $P_{O_2} = 1.6 \times 10^{-2}$ Torr [Fig. 5(b)]. This can be clearly seen from the histogram of the phase angles of the two specimens [Figs. 5(c) and 5(d)]. Comparing Figs. 5(c) and 5(d), it shows that the polarization reversal is less than 180° for the film deposited at $P_{O_2} = 1.6 \times 10^{-2}$ Torr and it suggests that the polarization switching is uncompleted. In addition, the numbers of domain on both directions are less than those in the film deposited at $P_{O_2} = 1.2 \times 10^{-4}$ Torr. These results indicate that the oxygen partial pressure during the film deposition has significant effects on polarization reversal. The different oxygen partial pressures most likely result in different concentrations of the oxygen vacancy in these two samples, and the oxygen vacancy may be the domain inversed center and can assist the polarization reversal, as suggested by Herng et al.[16] In addition, it was reported that the introduction of the oxygen concentration during deposition could reduce the amount of oxygen vacancies in the ZnO films.[35,36] The oxygen vacancy concentration was reduced with increasing oxygen partial pressure when the films were deposited in the oxygen deficient atmosphere.[37] Therefore, it is reasonable to believe that, for the undoped ZnO film samples, there are more oxygen vacancies in the film deposited under $P_{O_2} = 1.2 \times 10^{-4}$ Torr than that in the film deposited under $P_{O_2} = 1.6 \times 10^{-2}$ Torr. Here, the film deposited under $P_{O_2} = 1.6 \times 10^{-2}$ Torr shows a much more significant polarization switching behavior. Hence, the following discussions on possible RS mechanisms and the built-up schematic energy band diagrams as well as the Schottky barriers in Pt-tip/ZnO-film/Pt-bottom-electrode structures are all based on this assumption: i.e., there are more oxygen vacancies in the film deposited under low oxygen partial pressure. In fact, all of the observations can be well explained by this assumption. In this study, the polarization reversal are repeated at least five times on the same sample with the same tip but at different locations; it is also repeated by using the different tips on the same samples to eliminate the effects of wearing of the conductive coating of the tip or the changes of the tip geometry.

C. Correlation of RS behavior with the local charge distribution

KPFM technique is used to study the local charge characters in this work. First, the surface potential changes after a poling process (by tip bias) is measured by KPFM technique on the ZnO film deposited under $P_{O_2} = 1.2 \times 10^{-4}$ Torr. Figure 6(a) is the surface potential image after poling by 10 and −10 V tip biases in the adjacent two areas of 6×3 μm^2 within a 10×10 μm^2 scanned area. The scan rate is 0.5 Hz. It is generally known that the surface potential in the biased region included three types of charges, i.e., injection charge, screen charges, and polarization charges.[32,34] To quantitatively compare the KPFM results from different regions, the surface potential value of the unbiased region is reset to zero as in the previous studies[21,32,34] [Figs. 6(a)–6(f)]. If the region exhibits a larger surface potential value than that of the un-poled region, it means that the poled region is positive charged and vice versa. Figure 6(a) shows that the bright contrast in the region after poling by tip bias of 10 V, which indicates that the positive charges are stored in this region. Whereas the dark contrast in the region poled by tip bias of −10 V suggests that the surface potential value is smaller than that of the un-poled region and this means that the negative charges are stored in this region. As the injection charge and screen charge are related to the tip bias and the environments, such as adsorbed water molecules at the surface, ground tip scanning is conducted after the initial KPFM measurement. Figure 6(b) is the surface potential image after two times grounded-tip scans. It is obvious that the surface potential values in the two regions are changed significantly. The surface potential in the region poled by −10 V tip bias increases to the value similar to that of the un-poled region. This shows that the stored charges after poling by negative tip bias can be removed by grounded tip scanning and this suggests that the increased surface potential is most likely due to the surface screen charges rather than the polarization charges. In addition, as the grounded tip scanning may not be able to completely rule out the effects of adsorbed water molecules when the KPFM technique is conducted in the ambient air, the KPFM measurements are also conducted in the slow-flowing Ar environment after the sample was placed in a gas cell with Ar flowing for 2 h [Figs. 6(c) and 6(d)]. It is clear that the surface potential in the 10 V biased region (tip bias) is significantly reduced. This shows the increased surface potential after the positive biased in air is mainly due to the adsorbed water molecules. Whereas the surface potential in the negative biased region is also somewhat screened out by the water molecules. Next, as the c-AFM technique was conducted with sample bias (tip grounded), the effects of sample bias on the KPFM measurement is therefore studied, i.e., the poling process is conducted in air by using sample bias, and then the sample was placed in the gas cell with Ar flowing for 2 h and followed by the KPFM scanning in the slow-flowing Ar environments [Figs. 6(e) and 6(f)]. It is found that, unlike the case of poling process by tip bias, the effects of adsorbed water molecules to the poling by sample bias is much weaker, the KPFM measurements in Ar after 2 h still show higher surface potential on the region poled by −10 V sample bias

https://doi.org/10.1557/jmr.2015.310 Published online by Cambridge University Press

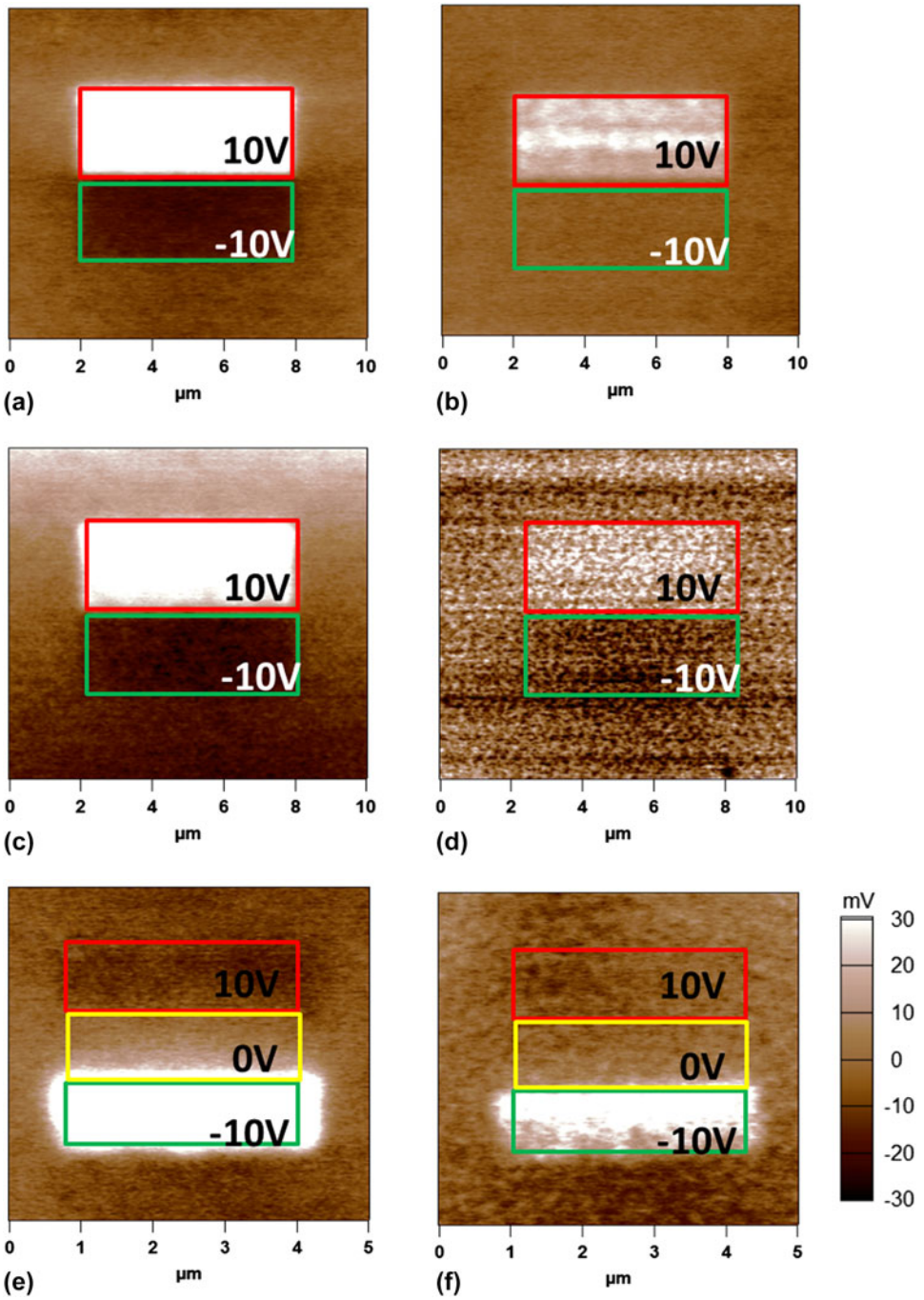


FIG. 6. Surface potential images for ZnO film deposited under $P_{O_2} = 1.2 \times 10^{-4}$ Torr: (a) after poling by 10 and −10 V tip biases in the two adjacent areas of 6 × 3 μm^2 within a 10 × 10 μm^2 scanning area in air; (b) the same region after two times grounded tip scanning in air; (c) after the same poling process as in (a) at another location in air; (d) after exposing sample to a flowing-Ar for 2 h; (e) after poling by 10, 0, and −10 V sample biases in three adjacent areas of 3 × 1 μm^2 within a 5 × 5 μm^2 scanning area in air; (f) the same region after exposing sample to slow flowing-Ar for 2 h. The surface potential values of the un-biased region in all of the images are reset to zero for comparison purpose.

(corresponding to 10 V tip bias). This result suggests that the effect of adsorbed water molecules during the KPFM measurements for the poling process by sample bias is very different from that of the tip bias. For the tip bias poling processes, especially under the positive bias, the increase of the surface potential is mainly due to the environmental effect, whereas for the sample poled by the negative sample bias, the effects of environmental is less significant. The surface potential is still higher after scanned in Ar environment.

https://doi.org/10.1557/jmr.2015.310 Published online by Cambridge University Press

D. Correlations between nonvolatile RS and polarization switching behavior as well as the charge distribution

After the confirmation that the way of biasing (tip or sample bias) has little effect on the polarization switching measurements, whereas there is a significant effect on the surface potential measurements, the sample bias is used in the subsequence studies. First, the c-AFM and KPFM techniques are applied to the same location (Fig. 7) to study the correlation between the RS behavior and local charge storage. Figures 7(a) and 7(b) are the topography and current images obtained by c-AFM technique. For this analysis, the sample surface is first poled with the sample biases of 10, 0, and −10 V on three adjacent areas of 3 × 1 μm^2 (enclosed by red lines), followed by c-AFM scan over a 5 × 5 μm^2 area with the sample bias of 0.5 V and the scan rate of 1 Hz. The same area is then scanned by KPFM mode. Figure 7(b) shows that the region poled by the −10 V sample bias has negligible current and hence it is HRS (blue color). On the other hand, the region poled by the 10 V sample bias is still at LRS, similar to that of the middle region (scanned with 0 V). Figure 7(c) is the corresponding surface potential images obtained by KPFM technique on the same area as that in Fig. 7(b). The region poled the −10 V sample bias exhibits a higher surface potential (bright contrast). The higher surface potential region has been extended beyond the boundary of the poling (−10 V) into the nearby region (poled by 0 V and unpoled region), however, there is no significant change on the surface potential in the region poled by the 10 V sample bias, which is consistent with the result shown in Fig. 6(e). Comparing Figs. 7(b) and 7(c), it is clear that the HRS region (poled by −10 V sample bias) shows a higher surface potential, however, there is no observable change in surface potential in the LRS region. As discussed before, the measured charges distribution also includes the polarization charges. Hence, the PFM measurement is then conducted on the same region to understand the function of the polarization charges during this process. Figures 7(d) and 7(e) are respectively the out-of-plane (vertical) PFM phase and amplitude images obtained on the same area after the c-AFM and KPFM measurements. It is clear that the PFM phase angle after poled by −10 V has switched from ~180° to approximately 0° in the HRS region [Fig. 7(f), obtained from the line profile (red) in Fig. 7(d)]. The spontaneous polarizations are switched to the downward direction toward the bottom electrode. In addition, it is also noticed that the PFM amplitude has increased significantly at the same region [Fig. 7(e)]. These results

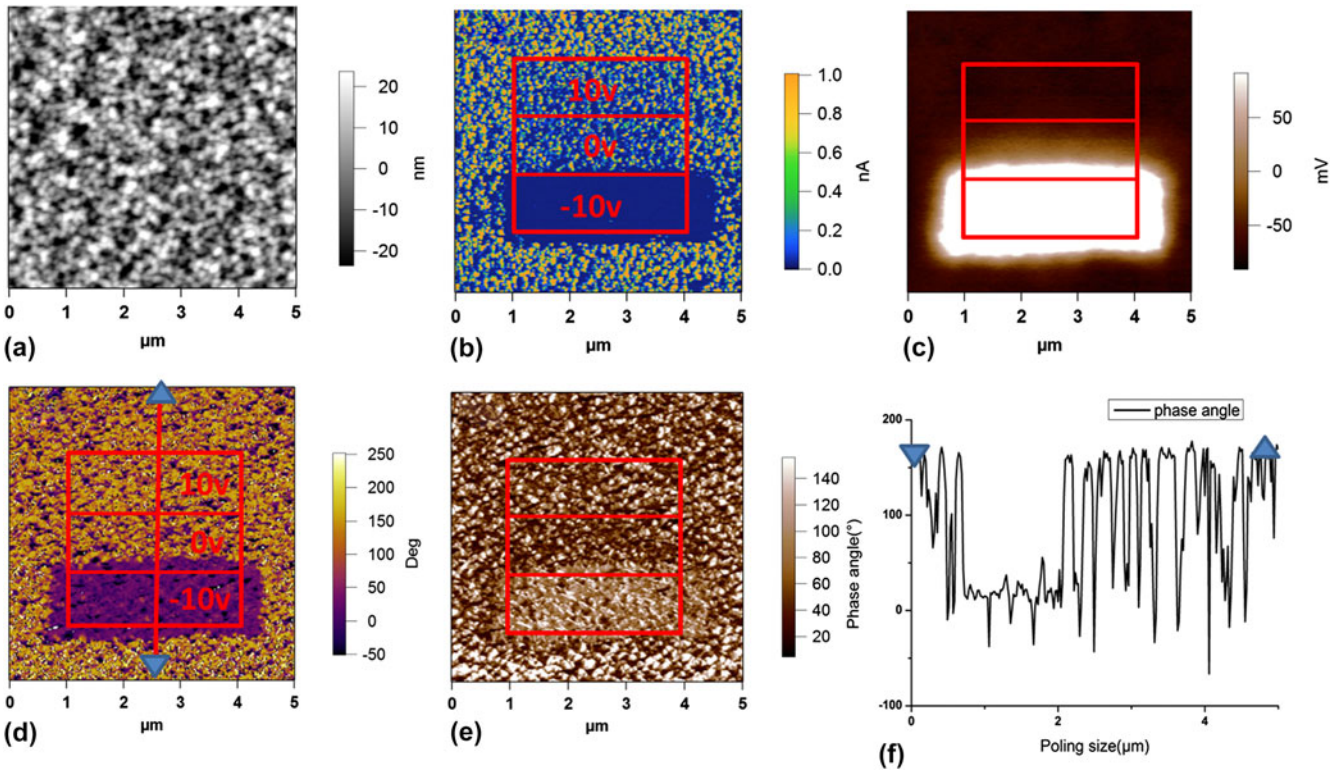


FIG. 7. Correlation between c-AFM, KPFM, and PFM images on undoped ZnO films deposited under $P_{O_2} = 1.2 \times 10^{-4}$ Torr: (a) topography; (b) current image after applying −10, 0, −10 V biases on the three adjacent areas of 3 × 1 μm^2 (enclosed by red lines); (c) corresponding surface potential image; (d) and (e) corresponding out-of-plane PFM phase and amplitude images; and (f) the line profiles of the out-of-plane PFM phase changes from the line section in (d).

https://doi.org/10.1557/jmr.2015.310 Published online by Cambridge University Press

suggest that the region poled by −10 V sample bias has switched to HRS, at the same time, the same region also shows a higher surface potential and a clear ~180° out-of-plane polarization switching. However, for the regions poled by sample biases of 0 or 10 V (LRS), there is no clear polarization-switching process. This result unambiguously confirms that the polarization switching behavior is related to the RS characteristics, and only HRS can show the polarization switching behavior in the un-doped ZnO thin films; this micro-scale observation also confirms the previous findings on global scale reported by Herng and colleagues.[16] In addition, it also suggests that the RS phenomena can be related to the charge storage capacity.

E. Discussions of RS mechanisms

We now discuss the possible RS mechanisms. The RS behavior may be due to several reasons: First, under external electric field, the formation of depletion region due to the Schottky barriers at the interfaces of Pt-tip/ZnO-film/Pt-bottom-electrode because of the different work functions of the contacting materials.[21] Second, as the uncompensated polarization may also affect the electronic conductance in the ferroelectric materials[25,38,39]; when the thin film thickness is relatively thin, the uncompensated polarization would affect the Schottky barrier since this uncompensated polarization can lead to a built-in filed, which may correspond to the order of a few MV/cm of the applied electric field and may increase the barrier's height,[39,40] and this may switch the sample to HRS. A recent work by Maksymovych and colleagues has confirmed that Fowerlor–Nordheim tunneling conductance was significantly reduced when the polarization vector was antiparallel to the applied electric field and this could lead the sample to HRS.[39] On the other hand, the Schottky barrier height might be decreased and the sample was then switched to LRS as the screening of the polarization charges.[39] Finally, the surface states of the samples or other environmental factors may also contribute to RS behavior as the experiment is conducted in the ambient condition.[38,41] Figures 8(a)–8(d) are the schematic energy band diagrams as well as the changes of the Schottky barriers at Pt-tip/ZnO-film/Pt-bottom-electrode structure due to the work function difference, depolarization electric field caused by uncompensated polarization, and the external electric field. Figure 8(a) is the energy band diagram in an ideal thermal equilibrium state of the Pt-tip/ZnO-film/Pt-bottom-electrode structure without the spontaneous polarization in ZnO film and external electric field. The symmetrical depletion region is due to the band bending resulting from the different work functions at the Pt/ZnO interfaces. Figure 8(b) is the modified energy band diagram with most upward spontaneous polarization in as-grown ZnO film and without external electric field. When ZnO film is deposited under deficient oxygen partial pressure, the bands will bend because of positively charged oxygen vacancies and the released electrons by oxygen vacancies.[17,38] Figure 8(b) shows that the released free electrons can compensate the positive polarization charges, $+Q_s$, and hence the band is bent downward, which can reduce the Schottky barrier height. On the other hand, the negative polarization charges, $-Q_s$, can be compensated by the positively charged oxygen vacancies. Hence the uncompensated polarization (P_E) can lead to a built-in field, $E_{built\text{-}in}$, oriented from positive polarization charges toward negative polarization charges. The band can be bended upward and hence the depletion region is affected by the concentration of V_O and the built-in field $E_{built\text{-}in}$ (Ref. 41). Figure 8(c) is the energy band diagram when poling with negative sample bias (e.g., −10 V) which is larger than the negative coercive bias and the polarization is switched to downward direction toward the bottom electrode. Both the migration/formation of positively charged oxygen vacancies and the switched downward polarization toward the bottom electrode interface can increase the width of the depletion region. These two factors together can switch the sample to HRS. In this case, the sample may behave similar to a capacitor. Hence, the positive charges can be stored in the sample, i.e., the formed V_O. Figure 8(d) is the energy band diagram in the structure when poling with positive sample bias (e.g., 10 V) and the polarization remains the same as that in the as-grown film. The forward bias at the Pt-bottom-electrode/ZnO interface may lead to Ohmic-like contact at this interface. In addition, there may be a large number of electrons injection at the Pt-tip/ZnO interface due to the reverse bias in this interface, this may screen the polarization effects, hence the polarization does not arouse a built in field antiparallel to the external electric field. Therefore, the sample is in LRS and significant current can be observed in this region (poled by positive bias).

This proposed RS mechanism is based on the c-AFM, KPFM, and PFM measurements on the same location. There are two possible sources of the surface charges in the KPFM measurement. The first is the migration/formation of the positively charged oxygen vacancies at the surface of the ZnO film, and/or holes injection into the ZnO film from the tip when the sample is under negative bias. Therefore, the surface potential by KPFM measurement shows a larger value. The second is that the negative charges in ZnO film can be attracted to and the positive charges can be repelled from the tip contacted area when the sample under negative bias.[8] In this case, the surface potential should show a smaller value. The results in this study have confirmed that after the poling process by the sample bias of −10 V, the samples are switched to HRS and the domains are switched to

https://doi.org/10.1557/jmr.2015.310 Published online by Cambridge University Press

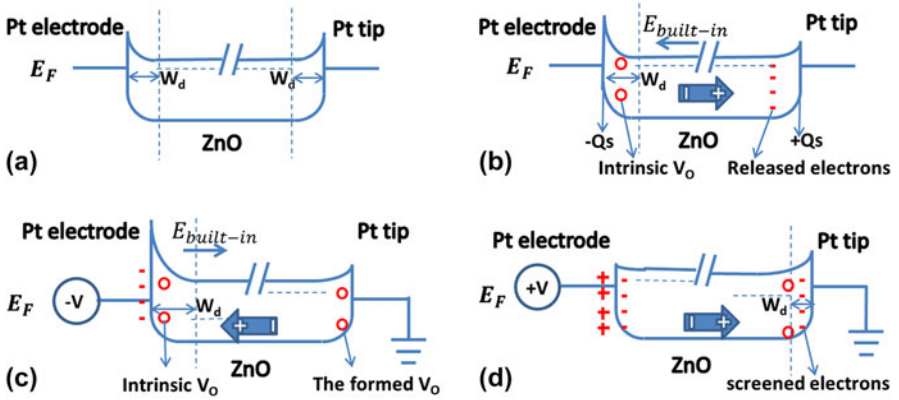


FIG. 8. Schematic energy band diagrams and Schottky barriers for Pt-tip/ZnO-film/Pt-bottom-electrode system: (a) in an ideal thermal equilibrium condition without the spontaneous polarization in ZnO film and external applied field; (b) modified band diagram with most upward spontaneous polarization in as-grown ZnO film and without external applied field; (c) when poling with negative sample bias (e.g., −10 V) and the polarization is switched to downward direction toward the bottom electrode; and (d) when poling with positive sample bias (e.g., 10 V) and the polarization remains the same as that in the as-grown film. In all of the figures, W_d indicates the width of the depletion region.

downward direction [Figs. 7(b) and 7(d)]. If there is no screen effect by the surface charge, the surface potential should be lower than that from the un-poled region. However, the KPFM measurements show the surface potential in this region is actually higher than that of the un-poled region [Figs. 6(e) and 7(c)], hence the polarization charges are likely screened by the positive charges; and therefore the first source is most likely dominated. Furthermore, comparing with the c-AFM current image [Fig. 7(b)], it can be confirmed that oxygen vacancy migration/formation is dominant over the holes injection effect. Since the ZnO thin film is in HRS within the negative poled region (poled by −10 V sample bias). If the effect of holes injection from tip is dominated, it should incur current flow. On the contrary, the migration/formation of the oxygen vacancies on the film surface, which may be the centers for domains reversal, can also assist polarization-switching process. In addition, as the downward polarization vector is antiparallel to the applied electric field and it can increase the Schottky barrier height, this can also switch the poled region to HRS [Fig. 8(c)]. Therefore, among the possible switching mechanisms, this oxygen-vacancy-related RS can simultaneously satisfy the c-AFM, KPFM, and PFM results. In the LRS, the electrons injection effect may be dominate. This is proved by the abruptly current changes [Fig. 7(b)]; in addition, there is no change in the polarization orientation when the sample is under 10 V sample bias [Fig. 7(d)].

The c-AFM, KPFM, and PFM measurements are also conducted on the same location on the undoped ZnO film deposited under $P_{O_2} = 1.6 \times 10^{-2}$ Torr. The poling processes are the same as before. The results are shown in Fig. S4. It is clear that the region poled by −10 V sample bias has also been switched to HRS, and the surface potential is also higher than that in the other regions. In addition, the domains in this region are also switched to downward direction in relative to the bias direction. However, it is also obvious that those changes are not as clear as those in the undoped ZnO film deposited at $P_{O_2} = 1.2 \times 10^{-4}$ Torr. Under the same condition, there are still some upward domains at the surface and have not been switched to downward direction. It is expected that the ZnO film deposited under higher oxygen partial pressure will have less amount of oxygen vacancies, therefore, the result reveals the oxygen vacancy plays an important role in the RS and polarization switching behavior in the ZnO film. Furthermore, the results also suggest that the ZnO film deposited under lower oxygen partial pressure can show a better RS and polarization switching behaviors.

IV. SUMMARY AND CONCLUSIONS

In summary, this work has shown the c-AFM current, PFM phase and amplitude, and KPFM surface potential images on the same location of the undoped ZnO thin film after the sample has been switched to HRS. The results have confirmed that the polarization switching is directly associated with the RS behavior. It also proves that when sample is in HRS, polarization switching can occur and the material shows the capability of charge storage. Furthermore, the RS mechanisms in ZnO film are proposed in term of oxygen vacancy assisted-switching and electronic conduction through the comparison of the PFM, KPFM, and c-AFM results. It is confirmed that the migration/formation of oxygen vacancy is dominant over the holes injection effect in the region poled by negative sample bias. However, in the LRS region, the electrons injection effect is dominated since there is an abruptly change of current when the applied sample bias is larger than the set voltage. Furthermore, the results

https://doi.org/10.1557/jmr.2015.310 Published online by Cambridge University Press

also confirm that the resistance switching behavior in ZnO thin films can be controlled by the oxygen partial pressure during the film deposition, the interfacial barriers at the bottom-electrode/sample and the tip/sample contact, as well as the uncompensated polarization in the samples.

REFERENCES

1. D.S. Jeong, R. Thomas, R.S. Katiyar, J.F. Scott, H. Kohlstedt, A. Petraru, and C.S. Hwang: Emerging memories: Resistive switching mechanisms and current status. *Rep. Prog. Phys.* **75**(7), 076502 (2012).
2. A. Sawa: Resistive switching in transition metal oxides. *Mater. Today* **11**(6), 28 (2008).
3. V. Garcia, S. Fusil, K. Bouzehouane, S. Enouz-Vedrenne, N.D. Mathur, A. Barthelemy, and M. Bibes: Giant tunnel electroresistance for non-destructive readout of ferroelectric states. *Nature* **460**(7251), 81 (2009).
4. K. Nagashima, T. Yanagida, K. Oka, M. Kanai, A. Klamchuen, J.S. Kim, B.H. Park, and T. Kawai: Intrinsic mechanisms of memristive switching. *Nano Lett.* **11**(5), 2114 (2011).
5. M. Bibes and A. Barthelemy: Multiferroics: Towards a magnetoelectric memory. *Nat. Mater.* **7**(6), 425 (2008).
6. J.F. Scott and C.A. Paz de Araujo: Ferroelectric memories. *Science* **246**(4936), 1400 (1989).
7. R.E. Fontana and S.R. Hetzler: Magnetic memories: Memory hierarchy and processing perspectives (invited). *J. Appl. Phys.* **99**(8), 08N902 (2006).
8. M.H. Lee and C.S. Hwang: Resistive switching memory: Observations with scanning probe microscopy. *Nanoscale* **3**(2), 490 (2011).
9. S.S.P. Parkin, K.P. Roche, M.G. Samant, P.M. Rice, R.B. Beyers, R.E. Scheuerlein, E.J. O'Sullivan, S.L. Brown, J. Bucchigano, D.W. Abraham, Y. Lu, M. Rooks, P.L. Trouilloud, R.A. Wanner, and W.J. Gallagher: Exchange-biased magnetic tunnel junctions and application to nonvolatile magnetic random access memory (invited). *J. Appl. Phys.* **85**(8), 5828 (1999).
10. I. Beinik, M. Kratzer, A. Wachauer, L. Wang, R.T. Lechner, C. Teichert, C. Motz, W. Anwand, G. Brauer, X.Y. Chen, X.Y. Hsu, and A.B. Djurišić: Electrical properties of ZnO nanorods studied by conductive atomic force microscopy. *J. Appl. Phys.* **110**(5), 052005 (2011).
11. W-Y. Chang, C-A. Lin, J-H. He, and T-B. Wu: Resistive switching behaviors of ZnO nanorod layers. *Appl. Phys. Lett.* **96**(24), 242109 (2010).
12. J.X. Xiao, W.L. Ong, Z. Guo, G.W. Ho, and K.Y. Zeng: Resistive switching and polarization reversal of Hydrothermal-method-grown undoped zinc oxide nanorods by using scanning probe microscopy techniques. *ACS Appl. Mater. Interfaces* **7**(21), 11412 (2015).
13. J. Song, Y. Zhang, C. Xu, W. Wu, and Z.L. Wang: Polar charges induced electric hysteresis of ZnO nano/microwire for fast data storage. *Nano Lett.* **11**(7), 2829 (2011).
14. J. Wang, Z. Song, K. Xu, and M. Liu: Rectifying switching characteristics of Pt/ZnO/Pt structure based resistive memory. *J. Nanosci. Nanotechnol.* **10**(11), 7088 (2010).
15. F.C. Chiu, P.W. Li, and W.Y. Chang: Reliability characteristics and conduction mechanisms in resistive switching memory devices using ZnO thin films. *Nanoscale Res. Lett.* **7**(1), 178 (2012).
16. T.S. Herng, A. Kumar, C.S. Ong, Y.P. Feng, Y.H. Lu, K.Y. Zeng, and J. Ding: Investigation of the non-volatile resistance change in noncentrosymmetric compounds. *Sci. Rep.* **2**, 587 (2012).
17. W.Y. Chang, Y.C. Lai, T.B. Wu, S.F. Wang, F. Chen, and M.J. Tsai: Unipolar resistive switching characteristics of ZnO thin films for nonvolatile memory applications. *Appl. Phys. Lett.* **92**(2), 022110 (2008).
18. J.J. Ke, Z.J. Liu, C.F. Kang, S.J. Lin, and J.H. He: Surface effect on resistive switching behaviors of ZnO. *Appl. Phys. Lett.* **99**(19), 192106 (2011).
19. B. Pérez-García, J. Zúñiga-Pérez, V. Muñoz-Sanjosé, J. Colchero, and E. Palacios-Lidón: Formation and rupture of Schottky nanocontacts on ZnO nanocolumns. *Nano Lett.* **7**(6), 1505 (2007).
20. J. Qi, M. Olmedo, J.G. Zheng, and J. Liu: Multimode resistive switching in single ZnO nanoisland system. *Sci. Rep.* **3**, 2405 (2013).
21. A. Kumar, T.S. Herng, K.Y. Zeng, and J. Ding: Bipolar charge storage characteristics in copper and cobalt co-doped zinc oxide (ZnO) thin film. *ACS Appl. Mater. Interfaces* **4**(10), 5276 (2012).
22. W.X. Li, L. Österlund, E.K. Vestergaard, R.T. Vang, J. Matthiesen, T.M. Pedersen, E. Lægsgaard, B. Hammer, and F. Besenbacher: Oxidation of Pt (110). *Phys. Rev. Lett.* **93**(14), 146104 (2004).
23. T.S. Herng, M.F. Wong, D. Qi, J. Yi, A. Kumar, A. Huang, F.C. Kartawidjaja, S. Smadici, P. Abbamonte, C. Sanchez-Hanke, S. Shannigrahi, J.M. Xue, J. Wang, Y.P. Feng, A. Rusydi, K.Y. Zeng, and J. Ding: Mutual ferromagnetic-ferroelectric coupling in multiferroic copper-doped ZnO. *Adv. Mater.* **23**(14), 1635 (2011).
24. C. Yang, J. Seidel, S. Kim, P. Rossen, P. Yu, M. Gajek, Y. Chu, L. Martin, M. Holcomb, and Q. He: Electric modulation of conduction in multiferroic Ca-doped $BiFeO_3$ films. *Nat. Mater.* **8** (6), 485 (2009).
25. A.Q. Jiang, C. Wang, K.J. Jin, X.B. Liu, J.F. Scott, C.S. Hwang, T.A. Tang, H.B. Lu, and G.Z. Yang: A resistive memory in semiconducting $BiFeO_3$ thin-film capacitors. *Adv. Mater.* **23**(10), 1277 (2011).
26. M.H. Lee, S.J. Song, K.M. Kim, G.H. Kim, J.Y. Seok, J.H. Yoon, and C.S. Hwang: Scanning probe based observation of bipolar resistive switching NiO films. *Appl. Phys. Lett.* **97**(6), 062909 (2010).
27. Y. Du, A. Kumar, H. Pan, K. Zeng, S. Wang, P. Yang, and A.T.S. Wee: The resistive switching in TiO_2 films studied by conductive atomic force microscopy and Kelvin probe force microscopy. *AIP Adv.* **3**(8), 082107 (2013).
28. A. Olbrich, B. Ebersberger, and C. Boit: Conducting atomic force microscopy for nanoscale electrical characterization of thin SiO_2. *Appl. Phys. Lett.* **73**(21), 3114 (1998).
29. S.V. Kalinin, A. Rar, and S. Jesse: A decade of piezoresponse force microscopy: Progress, challenges, and opportunities. *IEEE Trans. Ultrason. Ferroelectr. Freq. Control* **53**(12), 2226 (2006).
30. S.V. Kalinin, A.N. Morozovska, L.Q. Chen, and B.J. Rodriguez: Local polarization dynamics in ferroelectric materials. *Rep. Prog. Phys.* **73**(5), 056502 (2010).
31. S.V. Kalinin and D.A. Bonnell: Local potential and polarization screening on ferroelectric surfaces. *Phys. Rev. B.* **63**(12), 125411 (2001).
32. Y. Kim, C. Bae, K. Ryu, H. Ko, Y.K. Kim, S. Hong, and H. Shin: Origin of surface potential change during ferroelectric switching in epitaxial $PbTiO_3$ thin films studied by scanning force microscopy. *Appl. Phys. Lett.* **94**(3), 032907 (2009).
33. B.J. Jin, S.H. Bae, S.Y. Lee, and S. Im: Effects of native defects on optical and electrical properties of ZnO prepared by pulsed laser deposition. *Mater. Sci. Eng., B.* **71**(1–3), 301 (2000).
34. M.F. Wong, T.S. Herng, Z. Zhang, K.Y. Zeng, and J. Ding: Stable bipolar surface potential behavior of copper-doped zinc oxide films studied by Kelvin probe force microscopy. *Appl. Phys. Lett.* **97**(23), 232103 (2010).

https://doi.org/10.1557/jmr.2015.310 Published online by Cambridge University Press

35. H-W. Huang, C-F. Kang, F-I. Lai, J-H. He, S-J. Lin, and Y-L. Chueh: Stability scheme of ZnO-thin film resistive switching memory influence of defects by controllable oxygen pressure ratio. *Nanoscale Res. Lett.* **8**, 483 (2013).
36. Y. Ma, G.T. Du, T.P. Yang, D.L. Qiu, X. Zhang, H.J. Yang, Y.T. Zhang, B.J. Zhao, X.T. Yang, and D.L. Liu: Effect of the oxygen partial pressure on the properties of ZnO thin films grown by metalorganic vapor phase epitaxy. *J. Cryst. Growth* **255**(3–4), 303 (2003).
37. T.S. Herng, D.C. Qi, T. Berlijn, J.B. Yi, K.S. Yang, Y. Dai, Y.P. Feng, I. Santoso, C. Sánchez-Hanke, X.Y. Gao, A.T.S. Wee, W. Ku, J. Ding, and A. Rusydi: Room-temperature ferromagnetism of Cu-doped ZnO films probed by soft x-ray magnetic circular dichroism. *Phys. Rev. Lett.* **105**(20), 207201 (2010).
38. G.L. Yuan and J. Wang: Evidences for the depletion region induced by the polarization of ferroelectric semiconductors. *Appl. Phys. Lett.* **95**(25), 252904 (2009).
39. P. Maksymovych, S. Jesse, P. Yu, R. Ramesh, A.P. Baddorf, and S.V. Kalinin: Polarization control of electron tunneling into ferroelectric surfaces. *Science* **324**(5933), 1421 (2009).
40. A. Gruverman, D. Wu, H. Lu, Y. Wang, H.W. Jang, C.M. Folkman, M.Y. Zhuravlev, D. Felker, M. Rzchowski, C-B. Eom, and E.Y. Tsymbal: Tunneling electroresistance effect in ferroelectric tunnel junctions at the nanoscale. *Nano Lett.* **9**, 3539 (2009).
41. M. Qin, K. Yao, and Y.C. Liang: Photovoltaic mechanisms in ferroelectric thin films with the effects of the electrodes and interfaces. *Appl. Phys. Lett.* **95**(2), 022912 (2009).

Supplementary Material

To view supplementary material for this article, please visit http://dx.doi.org/jmr.2015.310.

https://doi.org/10.1557/jmr.2015.310 Published online by Cambridge University Press